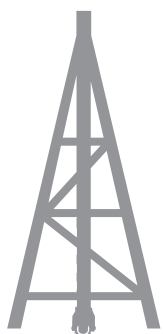
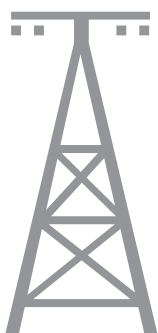
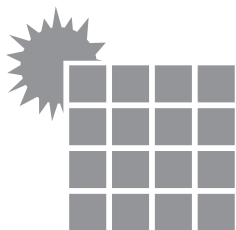


ISSN 2720-3581



# JOURNAL

OF GEOTECHNOLOGY  
AND ENERGY

FORMERLY AGH DRILLING, OIL, GAS

2022, vol. 39, no. 1



WYDAWNICTWA AGH

KRAKOW 2022

The “Journal of Geotechnology and Energy” (formerly “AGH Drilling, Oil, Gas”) is a quarterly published by the Faculty of Drilling, Oil and Gas at the AGH University of Science and Technology, Krakow, Poland. Journal is an interdisciplinary, international, peer-reviewed, and open access. The articles published in JGE have been given a favorable opinion by the reviewers designated by the editorial board.

## **Editorial Team**

### **Editor-in-chief**

Dariusz Knez, AGH University of Science and Technology, Poland

### **Co-editors**

Szymon Kuczyński  
Małgorzata Maria Formela  
Karol Dąbrowski  
Katarzyna Chruszcz-Lipska  
Rafał Matuła  
Sławomir Wysocki

### **Editorial Board**

Rafał Wiśniowski  
Danuta Bielewicz  
Stanisław Dubiel  
Andrzej Gonet  
Maciej Kaliski  
Stanisław Nagy  
Stanisław Rychlicki  
Jakub Siemek  
Jerzy Stopa  
Kazimierz Twardowski

### **Publisher**

AGH University Press

Linguistic corrector: *Aeddan Shaw*  
Technical editor: *Kamila Zimnicka*  
Desktop publishing: *Munda*  
Cover design: *Paweł Sepielak*

© Wydawnictwa AGH, Krakow 2022  
Creative Commons CC-BY 4.0 License  
ISSN: 2720-3581  
DOI: <https://doi.org/10.7494/jge>

Journal website: <https://journals.agh.edu.pl/jge>

---

Wydawnictwa AGH (AGH University Press)  
al. A. Mickiewicza 30, 30-059 Kraków  
tel. 12 617 32 28, 12 636 40 38  
e-mail: [redakcja@wydawnictwoagh.pl](mailto:redakcja@wydawnictwoagh.pl)  
[www.wydawnictwo.agh.edu.pl](http://www.wydawnictwo.agh.edu.pl)

---

# CONTENTS

---

Dariusz Knez, Herimitsinjo Rajaoalison, Donatille Nkunzi <b>Drilling mud influence on sandstone poroelastic parameters</b>	<b>5</b>
Oleksandr Kostyuk <b>Thermoelectric properties of pyrite in the supra-ore level of gold mineralization (Ukrainian Carpathians)</b>	<b>15</b>





Dariusz Knez

ORCID: 0000-0003-1028-2497

AGH University of Science and Technology, Faculty of Drilling, Oil and Gas, Krakow, Poland

Herimitsinjo Rajaoalison

ORCID: 0000-0002-4872-0109

AGH University of Science and Technology, Faculty of Drilling, Oil and Gas, Krakow, Poland

Donatille Nkunzi

ORCID: 0000-0003-1850-7304

AGH University of Science and Technology, Faculty of Drilling, Oil and Gas, Krakow, Poland

## DRILLING MUD INFLUENCE ON SANDSTONE POROELASTIC PARAMETERS

Date of submission:  
14.02.2022

Date of acceptance:  
18.02.2022

Date of publication:  
31.03.2022

© 2022 Authors. This is an open access publication, which can be used, distributed, and reproduced in any medium according to the Creative Commons CC-BY 4.0 License

<https://journals.agh.edu.pl/jge>

**Abstract:** Perhaps the most critical challenge faced during drilling operations is related to the stability of the well. Additionally, drilling mud plays a crucial role in wellbore stability, as one of its main uses is to support the wellbore wall during the drilling operation. However, ignorance of the effects of drilling mud on the mechanical properties of rock formation can also lead to well failure. The stability of the wellbore is also influenced by pore pressure during the drilling process. The analysis of changes in rock poroelastic parameters after drilling mud saturation was found to be useful regarding the abovementioned issues. Therefore, the measurement of the dynamic Young's modulus, Poisson's ratio and Biot's coefficient of sandstone samples was carried out to determine their trends of variations with confining pressure in different conditions such as dry, water and drilling mud filtrate saturation. The findings indicate that both the dynamic Young's modulus and the Poisson's ratio of the sandstone rock increased after saturation with water and drilling mud filtrate, while the Biot's coefficient was reduced. Furthermore, the velocity of the P wave, the dynamic Young's modulus and the dynamic Poisson's ratio of the sandstone rock were proportional to the confining pressure, while the Biot's coefficient were inversely proportional to the confining pressure. The results imply that effective stress calculation can be influenced by changes in poroelastic parameters established from geophysical measurements, and risk management of wellbore stability stability was increased.

**Keywords:** drilling mud, rock mechanical properties, Biot's coefficient, acoustic waves, dynamic measurement

# 1. Introduction

The drilling process is a very sensitive stage in the petroleum industry that influences the efficiency of exploration and production with high capital investments and risks. Better understanding of the formation that is being drilled is one way to avoid complications during this process. For example, knowing the effect of drilling mud on the geomechanical properties of rock formation is helpful in maintaining the stability of the well and minimizing complications during drilling operation. The disadvantage is that the chemical composition of the drilling fluid should be taken into account to avoid the chemomechanical interaction with the reservoir. Young's modulus, Poisson's ratio, and Biot's coefficient are fundamental parameters that effectively influence porous media. The pore pressure in the well is a key variable to maintain during the drilling process. The maintenance of well stability during drilling operations in oilfields requires knowledge of rock deformation and pore pressure behaviour [1]. Based on the values of parameters calculated near the wellbore stresses, controllable factors and proppants can be selected properly [2, 3]. The exact estimation of the subsurface pore pressure is crucial for successful well design and the reduction of operational costs and risks during the drilling process [4].

Drilling and production operations take place in porous media such as reservoirs saturated with different types of fluids including oil, gas, condensate, and water. For example, the compressibility of the rock decreases the pore pressure when fluid is injected into the rock. Permeability also influences the change in pore pressure where the latter increases in the presence of rock saturated with an impermeable liquid, while there is no occurrence of variation in pore pressure when the rock is permeable because the volume of injected water is equal to the volume flowing from the rock [5]. Therefore, the changes in pore pressure and volume of porous formation are the results of activities undertaken related to hydrocarbon production or even sequestration of carbon dioxide. These changes are very important because they can lead to formation compaction and subsidence expressed on the surface [6–8]. Therefore, understanding the Biot's coefficient that contributes to these changes is very important because this parameter is required in order to be able to predict the propagation of the pore pressure through the skeleton material. Therefore, the measurement of the Biot's coefficient is an important parameter for determining the poroelastic effect on porous rock, as it remains the essential poroelastic characteristic used to determine the effect of pore pressure that leads to a change in the effective stress of the rock formation and has a significant impact on the wellbore stability [9].

Overbalanced and underbalanced pressure are the most common cases encountered during drilling, especially in horizontal wells. Drilling mud density is used as a tool to balance wellbore pressure with formation pressure to avoid the loss of formation damage and wellbore breakouts [10, 11]. Formation damage is a usual circumstance that occurs at any stage of the oilfield cycle. It is caused by many factors such as clay swelling, the presence of solid hydrocarbons, and mainly filtrate blockage. This problem contributes to the low efficiency of the well. Therefore, the formulation of the drilling fluid should comply with the minimization of the invasion of the drilling mud solid, filtrate, and polymers into the formation. This is done by taking into account the amount of bridging agents and the viscosifier [12].

Therefore, understanding rock formation is a key factor in addressing these challenges, and this article describes the experimental results of the dynamic Young's modulus, Poisson's ratio and Biot's coefficient of sandstone rock formation as a function of hydrostatic stress using an acoustic velocity system in dry, water, and mud saturation.

# 2. Methodology

The studies of mechanical rock properties in this work are done dynamically using acoustic waves. The values of primary and secondary wave velocity and the density of the specimen are used to calculate these mechanical rock parameters. It is important to note that the dynamic moduli of the rock are different from the static moduli due to some assumptions before any calculation, such as homogeneous, isotropic and perfect elastic of the rock being studied, which is not always true in most cases [13]. The dynamic moduli of fine-grained and igneous rocks, as well as sedimentary rocks are higher than static moduli, including Young's modulus, shear modulus, and Poisson's ratio [14]. Furthermore, King's experimental studies on the anisotropy and nonlinearity of the mechanical behavior of rocks [14] supported such a differentiation between dynamic and static moduli due to randomly oriented cracks within the specimen. Therefore, the unconformities between the results of the measurement of dynamic and static elastic properties are mainly related to the variation of the lithology and microcrack distribution of microcracks in rock materials [15–17].

The dynamic mechanical properties of the rock were calculated using the ratio between the velocities of the P and S waves of the elastic wave through rock samples, using Newton's second law of motion and Hooke's law [18]. Therefore, the correlation between dynamic and static moduli depends on the adaptiveness of the

propagation of elastic wave and Hooke's law, as Newton's second law is always applicable. Multiple studies have been conducted on P-wave velocity, as it is very useful for various engineering purposes, such as weathering depth related to construction and formation saturation related to drilling process [19–21]. The sound velocity through the rock sample is affected by the rock type, density, grain size and shape, anisotropy, porosity, fluid content, stress, temperature, and pre-existing microfracture within the specimen. Furthermore, the effect of water content on the ultrasonic velocities through sandstone samples has been investigated by Wyllie et al., and they found that the velocity is decreasing as a function of saturation [22]. In addition, Kahraman derived some empirical relationship between the compressive velocity of dry and water-saturated rocks [23]. In the present work, the effects of different types of saturation fluids as well as the increase of confining pressure on the velocities of the compressional wave through sandstone rock will be investigated, together with the poroelastic parameters that relate to them.

An acoustic velocity system (AVS) is an apparatus used to measure the dynamic mechanical properties of rock samples using acoustic waves [24]. It is made up of a panel, core holder, pressure pipes, acoustic transducers and receivers, switch box, digital oscilloscope, hand pump, heating mantle, and a computer for data storage and analysis. The plugs were inserted into the coreholder in condition that axial is parallel (Fig. 1). A confining pressure of 7 to 45 MPa were applied to the system while the pore pressure valve was opened, which meant it was equal to atmospheric pressure. Thus, the pore pressure was constant throughout the measurement process.

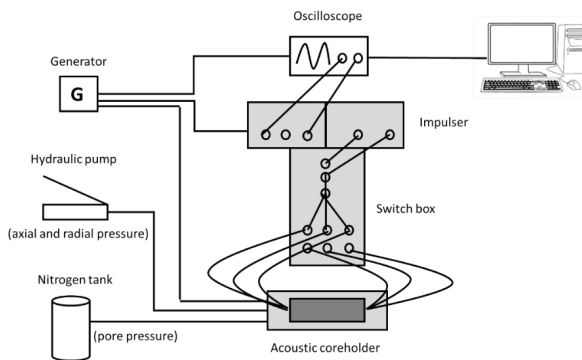


Fig. 1. AVS 1000 apparatus [25]

Acoustic wave velocities were measured to obtain geomechanical properties such as Young's modulus, Poisson's ratio. The low frequency transmitter and receiver were placed at each edge of the core holder and the time flight of P and S waves through the samples was recorded in microseconds [26]. Dynamic Young's modulus ( $E$ ), Poisson's ratio ( $\nu$ ) and the bulk modulus

were calculated using wave velocities and the density of sample using Equations (1), (2) and (3) [18, 27]:

$$\nu = \frac{V_P^2 - 2V_S^2}{2V_P^2 - V_S^2} \quad (1)$$

$$E = \frac{\rho V_S^2 (3V_P^2 - 4V_S^2)}{V_P^2 - V_S^2} \quad (2)$$

$$K = \frac{E}{3(1-2\nu)} \quad (3)$$

where  $\nu$  is the dynamic Poisson's ratio [–],  $E$  is the dynamic Young's modulus of the rock [Pa],  $\rho$  is the rock density ( $\text{kg/m}^3$ ),  $K$  is the bulk modulus of the rock [Pa],  $V_P$  is the compressional wave velocity [m/s], and  $V_S$  is the shear wave velocity [m/s].

The Biot's coefficient is calculated using the relationship between the rock and the bulk modulus. The dynamic bulk modulus is calculated from the P and S wave velocities obtained under in situ loading conditions. Biot's coefficient means the decrease of pore fluid induced by solid grains compaction. Biot's coefficient can be determined by Equation (4) [6, 7, 28, 29]:

$$\alpha = 1 - \frac{K_S}{K_O} \quad (4)$$

where  $K_S$  is the bulk modulus of the rock [Pa], and  $K_O$  is the bulk modulus [Pa].  $K_S$  can be calculated using Equation (5), while  $K_O$  is measured in hydrostatic load where the pore pressure must be equal to the confining pressure so that only the solid grains carry the confining pressure [24, 27]. Taking into account the homogeneity and isotropic nature of the samples studied, we used  $K_O = 85 \text{ GPa}$ , as it represents the volumetric bulk modulus for sandstone minerals [30].

$$K_S = \rho_{dry} V_P^2 - \frac{4}{3} \rho_{dry} V_S^2 \quad (5)$$

It is important to note that the value of the dynamic bulk modulus is different from the static bulk modulus due to the different strain amplitude of the experimental techniques [18, 31, 32].

## Experimental studies

The samples studied in this paper are cored from sandstone rock from an outcrop. The length and diameter of the samples were  $40 \text{ mm} \pm 1 \text{ mm}$  and  $38 \text{ mm}$ , respectively. The core samples were cut and polished according to the requirements to have a smooth surface, so the coupling between the transducer and the receiver will be good and the transit time measurement of the

arrival time of the waves will be more accurate, and the mechanical error due to the geometry of the sample will be minimized (Fig. 2). It is important to have as low a measurement error as possible because the uncertainty of the investigated poroelastic parameters influences many petroleum projects such as hydraulic fracturing [33, 34]. The P-wave velocity is then derived from the distance where the wave traveled (the sample length), divided by the pulse transit time. The samples obtained were kept in an oven at 70°C for at least a day to be dried and the weight of each sample was measured.



Fig. 2. Prepared core samples

Later, they were saturated with distilled water to calculate the bulk density and porosity. Water and drilling mud were used to saturate the samples in order to understand how the poroelastic properties behave with different types of fluid used, under incrementation of confining pressure. The results found are of 2.63 g/cm<sup>3</sup> and 13% respectively.

In all stages of the life of the well, including drilling, completion, stimulation, flow tests, production, and depletion, its stability is very important. During drilling operations, this is mainly concerned with the composition of the drilling mud and its density, so that the integrity of the wellbore is maintained without losing the drilling fluid. Failure occurs easily if one does not pay attention to the characteristics of the drilling mud and its effects on the formation being drilled [35, 36]. In this investigation, the drilling mud filtrate with chemical composition in Table 1 was used to saturate the sample to investigate its effect on the rock mechanical properties of the core samples under confining pressure.

Such research is very important to maximize the understanding of formation characteristics such as dynamic mechanical properties, which is necessary to formulate the mud weight window during drilling, so that the reservoir is economically productive and the costly problems induced by wellbore instabilities are reduced [37].

Table 1. Drilling mud composition

Material	Description	Quantity [%]
CMC	viscosifier	1.0
KCl	clay stabilizer	1.5
PHPA	–	0.3
CaCO <sub>3</sub>	alkalinity control/ mineral bridging agent	10.0
Organic bridging agent	–	1.0

### 3. Results and discussions

Understanding the stability issues during the drilling and production process is crucial, especially in case difficult geological conditions are encountered such as cross faults. The main cause of disasters and difficulties during drilling is related to poor understanding of the formation being drilled and the lack of adequate chemicals used to formulate the drilling mud. Worldwide, such disasters cost nearly 8 billion USD per year [38]. As part of preventive solutions, this study helps to understand the behaviour of the dynamic poroelastic parameters of the sandstone under variation of the confining pressure after saturation with water and drilling mud.

The first result shows the variation of the compressional velocity under the changed conditions. Next, the relationship between dynamic poroelastic parameters and confining pressure will be discussed, followed by an explanation of the possible reasons for the differentiation between the recorded values from water and mud-saturated samples. One of utilities of the understanding the dynamic mechanical properties of rock is its application to seismic response analysis. Dynamic shear strength and static strength are slightly different for hard rock, such as gneiss, but not necessarily the same for soft rock, such as sandstone, because it is affected by external and internal conditions, such as roughness, hardness, degree of weathering, and grain sizes [17, 24]. The compressional velocity through dry, water-saturated and mud-saturated sandstone samples, under increased confining pressure, is presented in Figure 3.

The increase in confining pressure results in linear increase of P-wave velocity, which is supported by the coefficient correlation of 0.94 for dry samples, while 0.86 and 0.99 for water and mud saturated samples, respectively. In addition, fluid saturation does affect the speed of the compression wave. It increases to 20% for water saturation and about 30% for drilling mud saturation (Fig. 3). It also shows the effects of saturation as well as the type of fluid on the velocity propagation of

compressional waves through porous media. The effect of the saturation of the water and mud filtrate on the

dynamic mechanical properties of the sandstone samples at room temperature is shown in Figure 4.

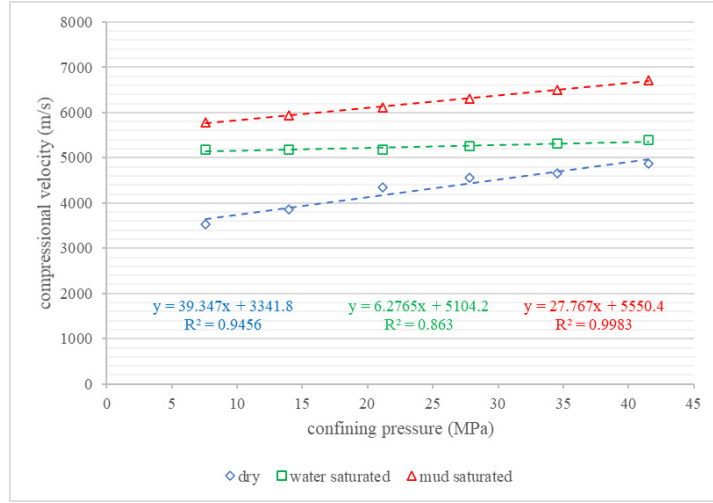


Fig. 3. Compressional velocity of dry, water-saturated and drilling mud saturated sandstone versus confining pressure

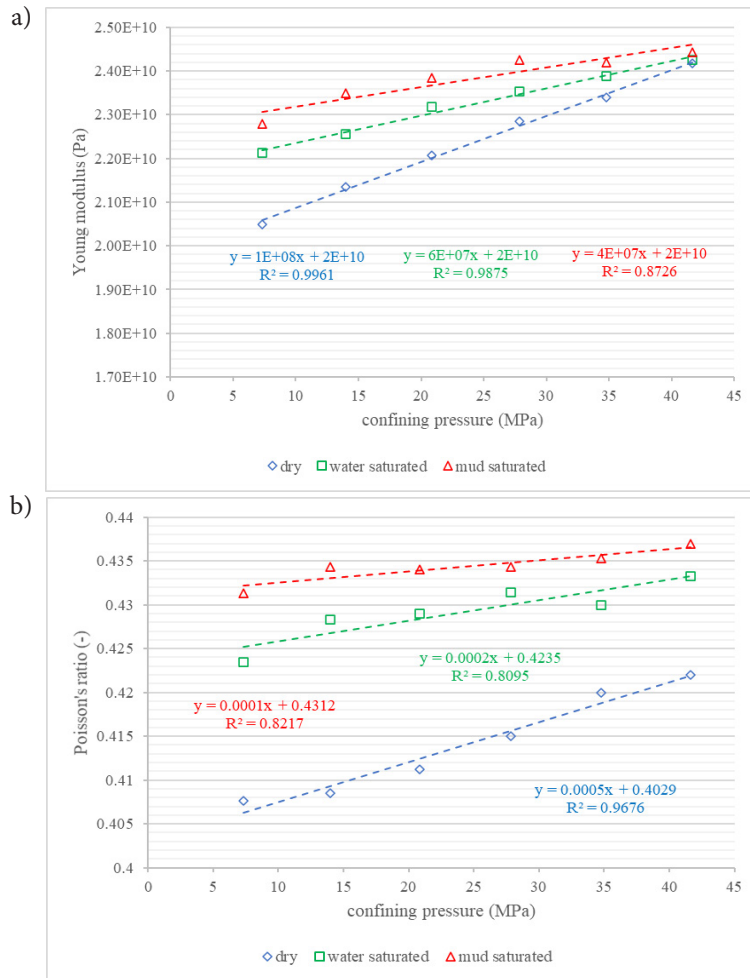


Fig. 4. Variation of Young's modulus (a) and Poisson's ratio (b), for dry, water saturated, and mud saturated sandstone versus confining pressure

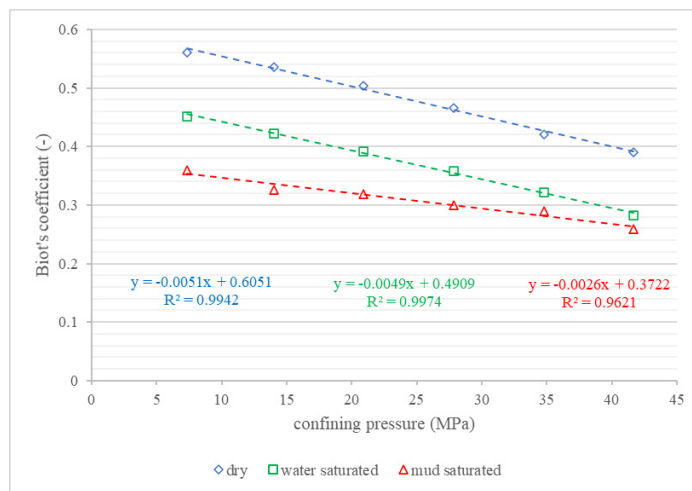


Fig. 5. Variation of the Biot's coefficient for dry, water-saturated, and mud-saturated sandstone versus confining pressure

The increase in the dynamic Young's modulus occurred after the sample was saturated with water. The results show that the sandstone core samples exhibit a slight increase in the Young's modulus behaviour up to 4%, 6.50% (Fig. 4a) and Poisson's ratio up to 5%, 6.10% (Fig. 4b) after being saturated with water and drilling mud filtrate, respectively. The increase is associated with the high viscosity of the drilling mud, which significantly increases the velocities of the P and S waves, which in turn increases both the Young's modulus and Poisson's ratio [39]. This contradicts what other studies have reported, namely that the drilling fluid weakens the rock due to the invasion of the loss of fluid with starch contained in the drilling mud [40] and the long exposure (24 hours) of samples with polymers that make up the drilling fluid, and this destroys the stiffness of the rock [41]. It is worth mentioning that the increase in the dynamic Young's modulus in this research does not mean an increase in the static Young's modulus value. Thus changes in the dynamic poroelastic parameters due to saturation could be different for static measurements. The Poisson's ratio increased slightly subsequently with the saturation of water and water-based drilling mud. Furthermore, the positive correlation between the Poisson's ratio, the Young's modulus, and confining pressure is supported by the significant correlation coefficient presented in Figure 4. In Figure 5, water saturation significantly decreased the dynamic Biot's coefficient of core samples by 23%.

Furthermore, the drilling of the mud filtrate has presented an important depletion of the Biot's coefficient of up to 35.40%. The negative linear correlation between Biot's coefficient and confining pressure is supported by the good correlation coefficient of 0.99 for dry samples, while 0.99 and 0.96 for saturated water and mud samples, respectively.

## 4. Conclusions

The effects of water and mud saturation on the poroelastic parameters of sandstone rock under increased confining pressure were carried out using acoustic waves. Laboratory results have shown the following:

1. The dynamic elastic modulus tends to increase when the rock is filled with fluids such as drilling mud and water due to the viscosity coupling phenomenon because the saturating drilling mud has high viscosity, which leads to an increase in wave velocities.
2. Samples filled with drilling mud slightly increase their dynamic Poisson's ratio and the Young's modulus when hydrostatic stress increases due to closure of microfractures within the sample and decreasing porosity.
3. When stress increases, there is a clear tendency to reduce the dynamic Biot's coefficient of cores saturated with water and drilling mud filtrate.
4. The Young's modulus and Biot's coefficient plots show convergence behaviour when hydrostatic stress increases.
5. An increase in the dynamic elastic modulus due to water and drilling mud saturation does not necessarily mean an increase in the static elastic modulus.

**Authors' Contributions:** All authors contributed to the acquisition of data and the writing of this manuscript. Conceptualization: Dariusz Knez, Herimitsinjo Rajaoalison; methodology: Dariusz Knez, Donatille Nkunzi; software: Herimitsinjo Rajaoalison, Donatille Nkunzi; validation: Dariusz Knez, Donatille Nkunzi, Herimitsinjo Rajaoalison; formal analysis, Dariusz Knez, Donatille Nkunzi, Herimitsinjo Rajaoalison; investigation: Donatille Nkunzi, Herimitsinjo Rajaoalison; resources: Dariusz Knez; data curation: Donatille

Nkunzi, Herimitsinjo Rajaoalison; writing – original draft preparation: Dariusz Knez, Donatille Nkunzi, Herimitsinjo Rajaoalison; writing – review and editing: Dariusz Knez, Donatille Nkunzi, Herimitsinjo Rajaoalison; supervision: Dariusz Knez; project administration: Dariusz Knez; funding acquisition: Dariusz Knez.

**Funding:** This research was funded by the AGH University of Science and Technology subsidy 16.16.190.779 and AGH–UNESCO.

**Conflicts of Interest:** The authors declare no conflict of interest.

## References

- [1] Suarez-Rivera R., Deenadayalu C., Chertov M., Hartanto R.N., Gathogo P., Kunjir R.: *Improving Horizontal Completions on Heterogeneous Tight-Shales*. Journal of Petroleum Technology, vol. 64, 2012, pp. 126–130. <https://doi.org/10.2118/1012-0126-JPT>.
- [2] Knez D., Wiśniowski R., Owusu W.A.: *Turning Filling Material into Proppant for Coalbed Methane in Poland – Crush Test Results*. Energies, vol. 12, 2019, 1820. <https://doi.org/10.3390/en12091820>.
- [3] Knez D., Calicki A.: *Looking for a New Source of Natural Proppants in Poland*. Bulletin of the Polish Academy of Sciences. Technical Sciences, vol. 66, no. 1, 2018, pp. 3–8. <https://doi.org/10.24425/119052>.
- [4] Mukerji T., Dutta N., Prasad M., Dvorkin J.: *Seismic Detection and Estimation of Overpressures. Part I: The rock physics basis*: CSEG Recorder, vol. 27, no. 7, 2002, pp. 34–57.
- [5] Kim K., Vilarrasa V., Makhnenko R.Y.: *CO<sub>2</sub> Injection Effect on Geomechanical and Flow Properties of Calcite-Rich Reservoirs*. Fluids, vol. 3, no. 3, 2018, 66. <https://doi.org/10.3390/fluids3030066>.
- [6] Biot M.A.: *General Theory of Three-Dimensional Consolidation*. Journal of Applied Physics, vol. 12, 1941, pp. 155–164. <https://doi.org/10.1063/1.1712886>.
- [7] Cheng A.-D.: *Material Coefficients of Anisotropic Poroelasticity*. International Journal of Rock Mechanics and Mining Sciences, vol. 34, 1997, pp. 199–205. [https://doi.org/10.1016/s0148-9062\(96\)00055-1](https://doi.org/10.1016/s0148-9062(96)00055-1).
- [8] Wang H.F.: *Quasi-Static Poroelastic Parameters in Rock and Their Geophysical Applications*. In: R.C. Liebermann, C.H. Sondergeld (eds.), *Experimental Techniques in Mineral and Rock Physics*, Pageoph Topical Volumes, Birkhäuser, Basel, pp. 269–286. [https://doi.org/10.1007/978-3-0348-5108-4\\_5](https://doi.org/10.1007/978-3-0348-5108-4_5).
- [9] Luo X., Were P., Liu J., Hou Z.: *Estimation of Biot's Effective Stress Coefficient from Well Logs*. Environmental Earth Sciences, vol. 73, 2015, pp. 7019–7028. <https://doi.org/10.1007/s12665-015-4219-8>.
- [10] Sloan J.P., Brooks J.P., Dear III S.F.: *A New, Nondamaging, Acid-Soluble Weighting Material*. Journal of Petroleum Technology, vol. 27, 1975, pp. 15–20.
- [11] Rajaoalison H., Knez D.: *Current Trends in Land Subsidence of the North-Central Part of Poland Using DInSAR Technique*. E3S Web Conferences, vol. 266, 2021, 03006. <https://doi.org/10.1051/e3sconf/202126603006>.
- [12] Vryzas Z., Matenoglou G., Kelessidis V.C.: *Assessment of Formation Damage Potential of Novel Drilling Fluids via Integration of Fluid Loss Data with Filter Cake Quality and Filtrate Core Penetration Depth from NMR and MRI*. Paper presented at the Abu Dhabi International Petroleum Exhibition & Conference, Abu Dhabi, UAE, November 2017, SPE-188544-MS, Society of Petroleum Engineers, 2017. <https://doi.org/10.2118/188544-MS>.
- [13] Ide J.M.: *The Elastic Properties of Rocks: A Correlation of Theory and Experiment*. Proceedings of the National Academy of Sciences of the United States of America, vol. 22, no. 8, 1936, pp. 482–496. <https://doi.org/10.1073/pnas.22.8.482>.
- [14] Tuman V.S., Alm R.F.: *Dynamic and Static Elastic Properties*. SPE-603-MS, Society of Petroleum Engineers, 1963.
- [15] King M.S.: *Static and Dynamic Elastic Moduli of Rocks under Pressure*. Paper presented at the 11<sup>th</sup> U.S. Symposium on Rock Mechanics (USRMS), Berkeley, California, June 1969, ARMA-69-0329, American Rock Mechanics Association, 1969.
- [16] Al-Shayea N.A., Khan K.: *Dynamic and Static Moduli of Limestone Rock from Saudi Arabia*. In: W. Sijing, F. Bingjun, L. Zhongkui (eds.), *Frontiers of Rock Mechanics and Sustainable Development in the 21st Century*. A.A.Balkema, 2001, pp. 109–113.
- [17] He J., Ling K., Wu X., Pei P., Pu H.: *Static and Dynamic Elastic Moduli of Bakken Formation*. Paper presented at the International Petroleum Technology Conference, Beijing, China, March 2019, IPTC-19416-MS, 2019. <https://doi.org/10.2523/IPTC-19416-MS>.
- [18] Fjær E.: *Static and Dynamic Moduli of a Weak Sandstone*. Geophysics, vol. 74, 2009, pp. 103–112. <https://doi.org/10.1190/1.3052113>.

- [19] Christaras B.: *P-Wave Velocity and Quality of Building Materials*. In: E. Yüzer, H. Ergin, A. Tugrul (eds.), *Industrial minerals and building stones: IMBS 2003: September 15–18, 2003 Istanbul Turkey*. IAEG, Istanbul 2003, pp. 295–300.
- [20] Christaras B., Mariolakos I., Foundoulis J., Athanasias S., Dimitriou A.: *Geotechnical Input for the Protection of Some Macedonian Tombs in Northern Greece*. In: *Proceedings 4th International Symposium on the Conservation of Monuments in the Mediterranean: new concepts, technologies and materials for the conservation and management of historic cities, sites and complexes: Rhodes, 6–11 May 1997*. Technical Chamber of Greece, Athens 1997, pp. 125–132.
- [21] Zezza F.: *Evaluation Criteria of the Effectiveness of Treatments by Non Destructive Analysis*. In: *Proceedings of the 2nd Course of CUN University. School of Monument Concervation*. Heraklion 1993, pp. 198–207.
- [22] Wyllie M.R.J., Gregory A.R., Gardner L.W.: *Elastic Wave Velocities in Heterogeneous and Porous Media*. *Geophysics*, vol. 21, 1956, pp. 41–70. <https://doi.org/10.1190/1.1438217>.
- [23] Kahraman S.: *The Correlations between the Saturated and Dry P-Wave Velocity of Rocks*. *Ultrasonics*, vol. 46, 2007, pp. 341–348. <https://doi.org/10.1016/j.ultras.2007.05.003>.
- [24] Rajaoalison H., Zlotkowski A., Rambolamanana G.: *Mechanical Properties of Sandstone Using Non-Destructive Method*. *Journal of Mining Institute*, vol. 241, 2020, pp. 113–117. <https://doi.org/10.31897/PMI.2020.1.113>.
- [25] Knez D., Rajaoalison H.: *Discrepancy between Measured Dynamic Poroelastic Parameters and Predicted Values from Wyllie's Equation for Water-Saturated Istebna Sandstone*. *Acta Geophysica*, vol. 69, 2021, pp. 673–680. <https://doi.org/10.1007/s11600-021-00543-3>.
- [26] Rao M.V.M.S., Prasanna Lakshmi K.J., Sarma L.P., Chary K.B.: *Elastic Properties of Granulite Facies Rocks of Mahabalipuram, Tamil Nadu, India*. *Journal of Earth System Science*, vol. 115, 2006, pp. 673–683. <https://doi.org/10.1007/s12040-006-0005-z>.
- [27] Rajaoalison H., Knez D., Zlotkowski A.: *Zmiany dynamicznych właściwości mechanicznych piaskowca istebniańskiego nasyconego solanką pod wpływem temperatury i naprężenia [Changes of dynamic mechanical properties of brine-saturated Istebna sandstone under action of temperature and stress]*. *Przemysł Chemiczny*, t. 98, nr 5, 2019, pp. 801–804. <https://doi.org/10.15199/62.2019.5.22>.
- [28] Franquet J.A., Abass H.H.: *Experimental Evaluation of Biot's Poroelastic Parameter Three Different Methods*. Paper presented at the Vail Rocks 1999, The 37th U.S. Symposium on Rock Mechanics (USRMS), Vail, Colorado, June 1999, ARMA-99-0349, American Rock Mechanics Association, 1999.
- [29] Salemi H., Iglauer S., Rezagholilou A., Sarmadivaleh M.: *Laboratory Measurement of Biot's Coefficient and Pore Pressure Influence on Poroelastic Rock Behaviour*. *The APPEA Journal*, vol. 58, no. 1, 2018, pp. 182–189. <https://doi.org/10.1071/AJ17069>.
- [30] Korsnes R., Christensen H.F., Trads N., Hiorth A., Madland M.V.: *Measuring the Biot Stress Coefficient and Its Implications on the Effective Stress Estimate*. Paper presented at the 47th U.S. Rock Mechanics/Geomechanics Symposium, San Francisco, California, June 2013, ARMA-2013-282, American Rock Mechanics Association, 2013.
- [31] Alam M.M., Borre M.K., Fabricius I.L., Hedegaard K., Røgen B., Hossain Z., Krogsbøll, A.S.: *Biot's Coefficient as an Indicator of Strength and Porosity Reduction: Calcareous Sediments from Kerguelen Plateau*. *Journal of Petroleum Science and Engineering*, vol. 70, 2010, pp. 282–297. <https://doi.org/10.1016/j.petrol.2009.11.021>.
- [32] Alam M.M., Christensen H.F., Fabricius I.L.: *Effective Stress Coefficient and Biot's Coefficient of Chalk from the Valhall Field, North Sea*. Paper presented at the EUROPEC/EAGE Conference and Exhibition, Amsterdam, The Netherlands, June 2009, SPE-121795-MS, Society of Petroleum Engineers, 2009. <https://doi.org/10.2118/121795-MS>.
- [33] Quosay A.A., Knez D., Ziaja J.: *Hydraulic Fracturing: New Uncertainty Based Modeling Approach for Process Design Using Monte Carlo Simulation Technique*. *PLOS ONE*, vol. 15, 2020, e0236726. <https://doi.org/10.1371/journal.pone.0236726>.
- [34] Quosay A.A., Knez D.: *Sensitivity Analysis on Fracturing Pressure Using Monte Carlo Simulation Technique*. *Oil Gas: European Magazine*, vol. 42, iss. 3, 2016, pp. 140–144.
- [35] Ramos G.G., Wilton B.S., Polillo A.F.: *Usage and Applicability of Pseudo-3D Stress Analysis in Borehole Stability Problems in Petroleum Drilling and Production Operations*. Paper presented at the 2nd North American Rock Mechanics Symposium, June 19–21, 1996, ARMA-96-1067, American Rock Mechanics Association, 1996.
- [36] Peng S., Fu J., Zhang J.: *Borehole Casing Failure Analysis in Unconsolidated Formations: A Case Study*. *Journal of Petroleum Science and Engineering*, vol. 59, iss. 3–4, 2007, pp. 226–238. <https://doi.org/10.1016/j.petrol.2007.04.010>.
- [37] Darvishpour A., Cheraghi Seifabad M., Wood D.A., Ghorbani H.: *Wellbore Stability Analysis to Determine the Safe Mud Weight Window for Sandstone Layers*. *Petroleum Exploration and Development*, vol. 46, iss. 5, 2019, pp. 1031–1038. [https://doi.org/10.1016/S1876-3804\(19\)60260-0](https://doi.org/10.1016/S1876-3804(19)60260-0).

- [38] Charlez P.A.: *The Concept of Mud Weight Window Applied to Complex Drilling*. Paper presented at the SPE Annual Technical Conference and Exhibition, Houston, Texas, October 1999, SPE-56758-MS, Society of Petroleum Engineers, 1999. <https://doi.org/10.2118/56758-MS>.
- [39] Khazanehdari J., Sothcott J.: *Variation in Dynamic Elastic Shear Modulus of Sandstone upon Fluid Saturation and Substitution*. *Geophysics*, vol. 68, 2003, pp. 472–481. <https://doi.org/10.1190/1.1567213>.
- [40] Cherblanc F., Berthonneau J., Bromblet P., Huon V.: *Influence of Water Content on the Mechanical Behaviour of Limestone: Role of the Clay Minerals Content*. *Rock Mechanics and Rock Engineering*, vol. 49, 2016, pp. 2033–2042. <https://doi.org/10.1007/s00603-015-0911-y>.
- [41] Lai B., Liang F., Zhang J., Li L., Liu H., Al-Muntasheri G.: *Fracturing Fluids Effects on Mechanical Properties of Organic Rich Shale*. Paper presented at the 50th U.S. Rock Mechanics/Geomechanics Symposium, Houston, Texas, June 2016, ARMA-2016-180, American Rock Mechanics Association, 2016.





Oleksandr Kostyuk

ORCID: 0000-0003-2218-1757

Ivan Franko State National University of Lviv, Lviv, Ukraine

## THERMOELECTRIC PROPERTIES OF PYRITE IN THE SUPRA-ORE LEVEL OF GOLD MINERALIZATION (UKRAINIAN CARPATHIANS)

**Abstract:** The thermoelectric properties of different-aged generations of pyrite from Lostun (Chyvchyny ore region) Tukalo and Kamin-Kliovka (Лостунь, Тукало, Камінь-Кльовка) (Rakhiv ore region) ore manifestations are investigated.

The research included traditional geological observations with the collection of samples of various hosting ores, together with mineralogical analysis measuring their reflective power and the thermo electro-motive force of pyrite.

Two pyrite generations (pyrite I and pyrite II) have been revealed by the investigation's results. The crystals belonging to the generations differ morphologically quite vividly (pyrite I has the form of a pentagonal dodecahedron, while pyrite II takes the form of a cube) and have different thermoelectrical properties. Pyrite I testifies to the fact that in the direction from the central parts of crystals with a pentagonal-dodecahedron tendency to its surface, the thermoelectrical properties essentially change. In particular, the central parts of pyrite I crystals have electron conductivity while its faces are mainly hole ones. Such essential changes of the pyrite thermoelectrical properties from the central parts of the crystals to their peripheral ones are probably mostly caused by quantitative changes of element admixtures in the crystalline lattice. However, the pyrite II thermoelectrical properties investigation results testify that this mineral has only hole-conductivity.

Thus, in terms of general thermo-e.m.f. (electromagnetic field) as well as selections range, the thermoelectric properties of the pyrite from the Lostun and Tukalo ore manifestations and the Sauliak (Сауляк) auriferous deposit are similar. The comparative character of the pyrite thermoelectric properties from the investigated ore manifestations, the Sauliak deposit and other auriferous deposits testify to the supra-ore level of the gold mineralization in Tukalo and Lostun objects and make it possible to assume that erosion shear of the gold mineralization in Tukalo ore manifestation is similar to the Sauliak deposit erosive shear and is deeper in comparison to the Lostun ore manifestation.

**Keywords:** pyrite, sulfides, gold, thermoelectroconductivity, ore manifestations

Date of submission:  
2.02.2022

Date of acceptance:  
28.02.2022

Date of publication:  
31.03.2022

© 2022 Author. This is an open access publication, which can be used, distributed, and reproduced in any medium according to the Creative Commons CC-BY 4.0 License

<https://journals.agh.edu.pl/jge>

## 1. Introduction

The Chyvchyny (Чивчини) and Rakhiv (Рахів) ore regions have some common features in terms of geological structure (structural-tectonic, petrological, lithology-stratigraphic [1–5]. Their structural-metallgenetic position is caused by belonging to the Chyvchyny and Rakhiv outcrops of the Marmarosky massif. The single-type ore-bearing formations are spread within its boundaries.

In the Rakhiv ore region in particular, the following objects are known: the Sauliak auriferous deposit, and the Bilyi Potik (Білий Потік), Kamin-Kliovka, Tukalo, Velykiy Banskiy (Великий Банський), Yaseniv (Ясенів) ore manifestations. Within the Chyvchyny ore region are found the Albin (Альбин), Dobryn (Добрин), Lostun, Mokryn (Мокрин), Perkalab (Перкалаб), Preluchnyi (Прелучний) and Popadynets (Попадинець) ore manifestations.

In our previous scientific papers we presented data concerning the typomorphism of minerals-semiconductors from the Bilyi Potik, Velykiy Banskiy [6, 7] Dobryn and Albin [6, 8] and Kamin-Kliovka ore manifestations [9].

So far as the Tukalo, Lostun and Kamin-Kliovka ore manifestations are similar in terms of their geological formation conditions and mineral composition [10], we considered a more detailed study and comparison of the peculiarities of physical-chemical conditions of mineralization worthwhile.

The thermoelectric properties of different-aged generations of pyrite from Lostun (Chyvchyny ore region), Tukalo and Kamin-Kliovka (Rakhiv ore region) ore manifestations are investigated in this paper.

Data ( $SR-\alpha_{med}$ ) testifies to the functional connection of the average values ( $\alpha_{med}$ ) of statistically reliable selections of thermo-e.m.f. (hole or electron conductivity) with ranges of these selections (SR). It provides an opportunity to reflect not only the peculiarities of the thermo-e.m.f. properties of the mineral different generations but also different parts of the separate crystals and (be thermo-e.m.f. vector) evaluate the changes and tendencies acquired during its formation).

The comparative character of the pyrite thermoelectric properties from the investigated ore manifestations, the Sauliak deposit and other auriferous deposits can testify to the supra-ore level of the gold mineralization in the Tukalo, Kamin-Kliovka (Fig. 1) and Lostun objects, and make it possible to assume that the erosion shear of the gold mineralization in the Tukalo ore manifestation are similar to the Sauliak deposit erosive shear and is deeper in comparison to the Lostun ore manifestation.

## 2. Methods

Thermo-e.m.f. was determined with the help of apparatus assembled in an applied thermobarogeochemistry laboratory. The main measuring instrument was a V7-21 microvoltmeter. Also employed were electrodes-needles that made it possible to thermally excite every area of the surface of the investigated samples. The tension directed to a hot electrode was stabilized with the help of a VIP-10 feeding block. The precision and stability of measurements was checked by the periodic measurement of standard thermo-e.m.f. (a constantans plate produced from a copper-constant thermocouple) and by supporting the constant difference value between the working surfaces of the hot and cold electrodes (100°C) with a help of potentiometric control. Therefore the possible systematic error of thermo-e.m.f. measurement was minimized. The measured potential difference between the excited and unexcited parts of the investigated mineral-semiconductor was divided into the difference of temperature between the working surfaces of the hot and cold electrodes. The coefficient of thermoelectric potential  $\alpha$  of investigated sample were brought to 1 degree (mcV/deg) and were plotted onto corresponding diagrams. Grouping intervals of thermo-e.m.f. values were picked out in conformity with known empiric stredges Formula (1):

$$\alpha = \frac{(\alpha_{max} - \alpha_{min})}{1 + 3.332 \log n} \quad (1)$$

where:

$\alpha_{max} - \alpha_{min}$  – selection range,  
 $n$  – quantity of measurements.

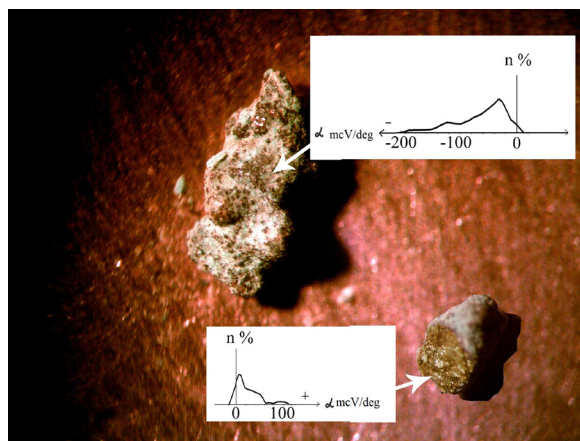


**Fig. 1.** Method for the determination of power thermo-e.m.f. 50 measurements of thermo-e.m.f. value were realized in both the central part of pyrite grains and on its surfaces or separate faces (ore manifestation Kamin-Kliovka, magnification power 12.5 ×)

Every investigated crystal or mineral grain was tested 50 times; only very fine grains in separate cases were studied by fewer measurements. 50 measurements of thermo-e.m.f. values were realized in both the central part of crystals, the grains and on its surfaces or separate faces (Fig. 1).

### 3. Results

#### 3.1. Lostun ore manifestation

The Lostun ore manifestation is situated 600 m to the south-east of the Lostun mount within the Chyvchynty ore region and occurs in chlorite-quartz( $\text{SiO}_2$ ) and sericite-chlorite-quartz shists that form the core of the anticline fold of the north-western strike. The rocks are greatly folded and complicated by forms of a superior order.

According to Matkovsky's data [5], lead-zinc mineralization within this ore manifestation is connected with brecciate rocks consisted of fragments of sericite-quartz and sericite-chlorite slates, sometimes with barite, barite-quartz and quartz-barite-carbonate veined formations.

The main minerals of the ore manifestation (Tab. 1) form the following mineral associations: chlorite-quartz, sericite-quartz, sericite-chlorite-quartz, pyrite-quartz, pyrite-galenite-sphalerite, pyrrhotite-chalcopryrite-quartz, quartz-carbonate-barite.

The main ore mineral of this ore manifestation is galenite, in close association with sphalerite, pyrite and chalcopryrite. As a rule, these minerals form fine impregnations, small (to 5 mm) bunches and thin streaks of different sizes (from 0.1 to 2.5–3.5 mm).

In disintegrated rocks, blocks within the ore manifestation boundaries were observed as fragments of ore bodies, where some galenite separations reach 5–7 sm (centimeters) in size, while chalcopryrite – 3–4 sm and pyrite – 2–3 sm.

**Table 1.** Main minerals of the Lostun ore manifestation

Non-metalliferous	Ore
Quartz I, II, III	pyrite I, II
Chlorite	pyrrhotite
Sericite	chalcopryrite
Barite	galenite
Carbonate I, II	sphalerite

The pyrite is widespread, not only in the ore bodies but also in enclosed rocks and was studied in detail. In particular, these mineral forms separations in enclosed rocks in the form of separate crystalline individuals (to 7 mm in size) and separations of an irregular form (10–15 mm in size). In the quartz streaks, pyrite has a tendency be connected with its selvage parts but may occur in the quartz in the form of impregnations, thin streaks and irregular separations. The general selection of the pyrite thermo-e.m.f. values in the Lostun ore manifestation are presented in Figure 2b.

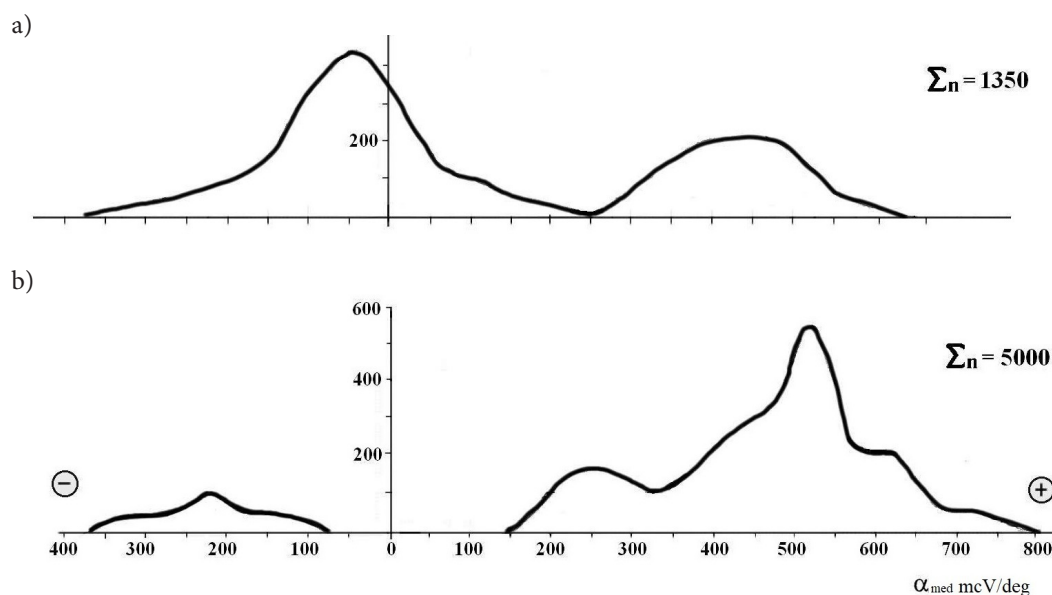


**Fig. 2.** General selections of thermo-e.m.f. values of pyrite from the Sauliak deposit (a) – upper part [10] and Lostun (b) – lower part;  $\Sigma n$  – measurements quantity

Two pyrite generations (pyrite I and pyrite II) have been revealed by the investigation. The crystals belonging to the generations differ morphologically quite vividly (pyrite I has the form of a pentagonal dodecahedron, while pyrite II takes the form of a cube) and have different thermoelectrical properties.

### 3.2. Tukalo ore manifestation

The Tukalo ore manifestation is situated 700 m above the Tukalo stream junction (a left tributary of the Tysa (Тиса) ) on the outskirts of Dilove (Ділове) village in the Rakhiv ore region. The main minerals of the ore manifestation (Tab. 2) form the following mineral associations: chlorite-quartz, sericite-quartz, pyrite-quartz, pyrite-galenite-sphalerite). Gold mineralization is spatially connected with an intensive schist formation zone. A ferruginated and intensive silicified gold-bearing zone is situated among the chlorite-sericite-quartz slates. Numerous mainly fine quartz streaks with a thickness to the first centimeters (except quartz and carbonate) and contain galenite, pyrite, chalcopyrite and native gold. These minerals are also superimposed onto enclosed rocks forming its impregnated or streaky-impregnated texture.

**Table 2.** Main minerals of the Tukalo ore manifestation

Non-metalliferous	Ore
Quartz I, II, III	pyrite I, II
Chlorite	galenite
Sericite	sphalerite
Carbonate I, II	chalcopyrite

A general selection of the pyrite thermo-e.m.f. values in the Tukalo ore manifestation are presented in Figure 3b.

Two pyrite generations (pyrite I and pyrite II) were revealed by the investigation. The crystals belonging to the generations differ morphologically quite vividly (pyrite I has the form of an octahedron, while pyrite II takes the form of a cube) and have different thermoelectrical properties.

### 3.3. Kamin-Kliovka ore manifestation

The Kamin-Kliovka ore manifestation is situated 300 m from the Kamin-Kliovka mountain on the outskirts of the city of Rakhiv. The main minerals of the ore manifestations (Tab. 3) form the following mineral associations: chlorite-quartz, sericite-quartz, quartz-barite-carbonate, pyrite-quartz, pyrite-galenite-sphalerite).

Two pyrite generations (pyrite I and pyrite II) have been revealed by the investigation. The crystals belonging to the generations differ morphologically quite vividly (pyrite I has the form of an octahedron, while pyrite II takes the form of a cube) and have different thermoelectrical properties.

**Table 3.** Main minerals of the Kamin-Kliovka ore manifestation

Non-metalliferous	Ore
Quartz I, II	pyrite I, II
Carbonate II	pyrite I, II
Quartz II	sphalerite

As a rule, pyrite I thermo-e.m.f. values fluctuate from -500 to +980 change from 120 to 480 mcV/deg (Tab. 4).

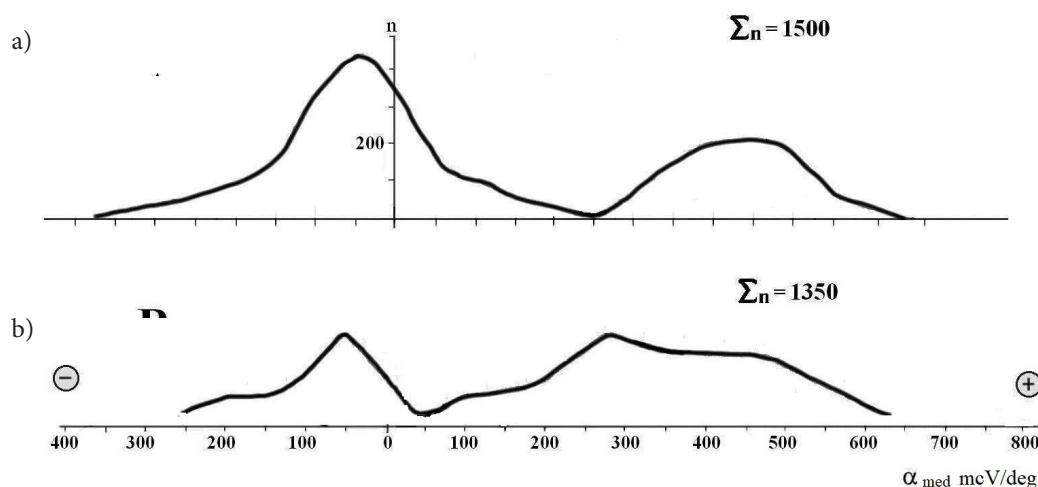


**Fig. 3.** General selections of thermo-e.m.f. values of pyrite from Sauliak deposit (a) – upper part [10] and Tukalo (b) – lower part);  $\Sigma n$  – measurements quantity

**Table 4.** Pyrite I and II thermo-e.m.f. values for the Lostun ore manifestation in the inner parts of crystals (a) and their faces (b)

Crystal number	Simple forms that determine crystal habit	Pyrite generations	$\alpha$ [mV/deg]			Selection range [mV/deg]
			max.	min.	average	
1 (a)	cube	II	+580	+270	+444	310
1 (b)	cube	II	+670	+270	+460	400
2 (a)	cube	II	+590	+250	+402	340
2 (b)	cube	II	+600	+370	+508	230
3 (a)	cube	II	+610	+320	+435	290
3 (b)	cube	II	+1000	+690	+829	310
4 (a)	pentagonal dodecahedron	I	-390	-100	-235	290
4 (b)	pentagonal dodecahedron	I	+790	+510	+620	280
5 (a)	cube	II	+460	+170	+304	290
5 (b)	cube	II	+750	+470	+594	280
6 (a)	pentagonal dodecahedron	I	+580	+100	+277	480
6 (b)	pentagonal dodecahedron	I	+760	+400	+622	360
7 (a)	cube	II	+600	+320	+476	280
7 (b)	cube	II	+600	+390	+515	210
8 (a)	cube	II	+680	+280	+437	400
8 (b)	cube	II	+810	+410	+610	400
9 (a)	cube	II	+590	+320	+460	270
9 (b)	cube	II	+560	+220	+356	340
10 (a)	pentagonal dodecahedron	I	-500	-150	-315	350
10 (b)	pentagonal dodecahedron	I	+790	+380	+588	410
11 (a)	cube	II	+520	+200	+382	320
11 (b)	cube	II	+620	+370	+514	250
12 (a)	cube	II	+560	+260	+268	300
12 (b)	cube	II	+640	+440	+525	200
13 (a)	cube	II	+590	+280	+465	310
13 (b)	cube	II	+620	+390	+538	230
14 (a)	pentagonal dodecahedron	I	-170	-50	-109	120
14 (b)	pentagonal dodecahedron	I	+380	+180	+280	200
15 (a)	cube	II	+450	+210	+323	240
15 (b)	cube	II	+630	+420	+531	210
16 (a)	cube	II	+640	+280	+438	360
16 (b)	cube	II	+660	+370	+514	290
17 (a)	cube	II	+610	+150	+399	460
17 (b)	cube	II	+780	+500	+632	280
18 (a)	pentagonal dodecahedron	I	+600	+200	+415	400
18 (b)	pentagonal dodecahedron	I	+980	+600	+710	380
19 (a)	cube	II	+350	+140	+229	210
19 (b)	cube	II	+610	+370	+504	240
20 (a)	pentagonal dodecahedron	I	-500	-150	-282	350
20 (b)	pentagonal dodecahedron	I	+640	+320	+454	320
21 (a)	pentagonal dodecahedron	I	+630	+370	+542	260
21 (b)	pentagonal dodecahedron	I	+650	+480	+587	170
22 (a)	cube	II	+300	+100	+206	200
22 (b)	cube	II	+560	+200	+420	360
23 (a)	cube	II	+350	+140	+238	210
23 (b)	cube	II	+610	+370	+524	240
24 (a)	pentagonal dodecahedron	I	-320	-100	-229	220
24 (b)	pentagonal dodecahedron	I	+730	+350	+551	380

Variational curves of the distribution of the thermo-e.m.v. values for the greater part of the investigated crystals are bimodal. Such a peculiarity can be explained by the probable later growth of the peripheral parts of some of the mineral crystals from a later fluid portion. The pyrite I diagram ( $SR-\alpha_{med}$ ) (Fig. 4) testifies to the fact that in the direction from the central parts of crystals of a pentagonal-dodecahedron habit to their surface, the thermoelectrical properties essentially change. In particular, the central parts of pyrite I crystals have electron conductivity while its faces are mainly hole ones. Such essential changes to the thermoelectrical properties of the pyrite from the central parts of crystals to their peripheral ones are probably caused by quantitative changes in the element admixtures in the crystalline lattice. Data ( $SR-\alpha_{med}$ ) testifies to the functional connection of the average values ( $\alpha_{med}$ ) of statistically reliable selections of thermo-e.m.f. (hole or electron conductivity) with ranges of these selections (SR). It provides the opportunity to not only reflect on the peculiarities of the thermo-e.m.f. properties of the

mineral different generations, but also different parts of the separate crystals and (be thermo-e.m.f. vector) evaluate the changes in the tendencies acquired during its formation).

The pyrite II thermoelectrical properties results testify to the fact that this mineral has only hole-conductivity. All thermo-e.m.f. values fluctuate from +200 to +600 mcV/deg. The selection range of the pyrite II thermo-e.m.f. values are about +210 to -4600 mcV/deg. Variational curves of the general selections of thermo-e.m.f. values for many pyrite crystals (especially crystals with intensive striation of the faces) have bimodal similarity with scarcely noted excesses that are probably caused by initial and later growth of this pyrite generation from different "waves" of the same fluids.

Diagram ( $SR-\alpha_{med}$ ) of the pyrite II (Fig. 5) testifies to the fact that in the direction from the central parts of the cubic habit crystals to their surface, the thermoelectrical properties change from low meanings of the hole conductivity to superior ones, that is in this case one can only see quantitative changes to the thermo-e.m.f. values.

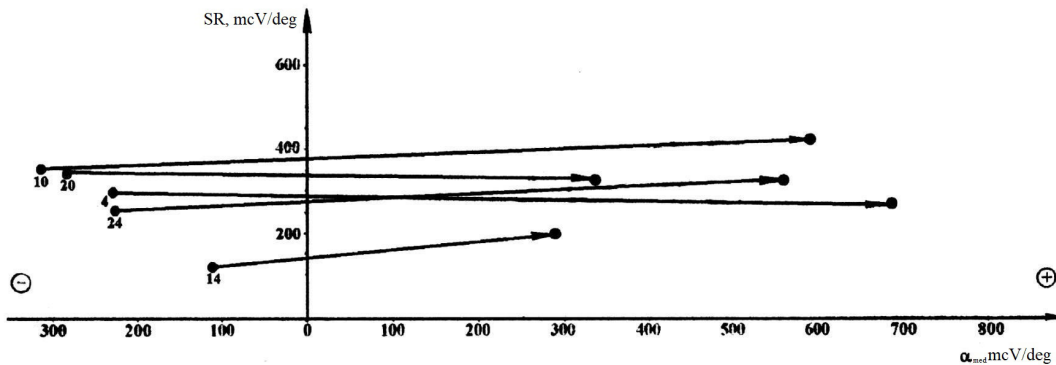


Fig. 4. Thermo-e.m.f. vectors of the pyrite I thermo-e.m.f. average values alterations (vectors of the crystals growth) in direction from central parts of crystals with a pentagonal dodecahedral habit to their surface (Lostun, Chyvchyny ore manifestation)

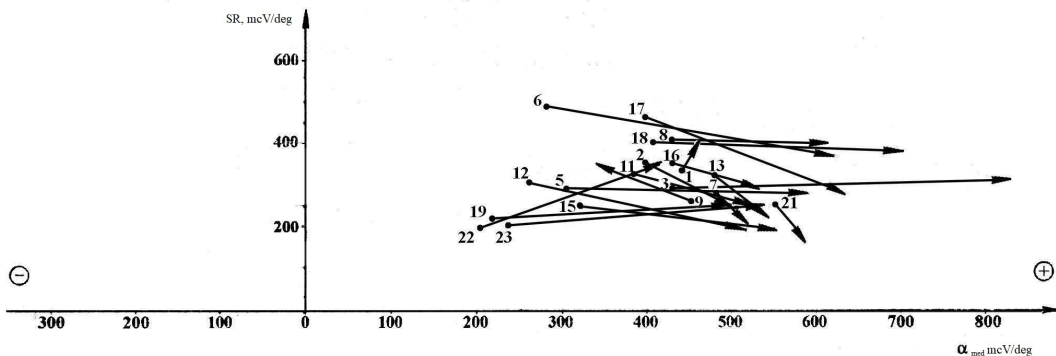


Fig. 5. Thermo-e.m.f. vectors of the pyrite II thermo-e.m.f. average values alterations (vectors of the crystals grown in direction from the central parts of the cubic habit crystals to their surface (Lostun, Chyvchyny ore manifestation)

With the Tukalo and Kamin-Kliovka manifestations, the thermoelectrical pyrite properties from quartz streaks in enclosed rocks were investigated in detail (Tab. 5).

A general selection of pyrite thermo-e.m.f. values from the Tukalo ore manifestation are presented in Figure 3. According to their morphology and size, the pyrite crystals from this ore manifestation are scarcely distinguished so far as their habit is mainly determined by cube and octahedron combination. At the same time, the results of investigations of the thermoelectric properties of pyrite crystalline samples the opportunity to assume that its generation, growth and later growth took place in a different manner. In particular, the general selection of thermo-e.m.f. values testifies to the presence of an obvious bimodal distribution of these parameters while thermo-e.m.f. vectors in  $SR-\alpha_{med}$  diagram are oriented in a different manner: in one case, in direction from electron conductivity to hole conductivity (or from low values of hole conductivity to higher ones): in another case –

from higher values of hole conductivity to lower (or to the electron meanings) (Fig. 6).

Thus, by general thermo-e.m.f. as well as selections range, the thermoelectric properties of the pyrite from Lostun, Kamin-Kliovka, and Tukalo ore manifestations and the Sauliak auriferous deposit (Tab. 6) are similar (in particular, by statistically reliable selections of thermo-e.m.f. values investigated crystals possess electron, hole or mixed conductivity; at the same time these meanings are clearly grouped into two massifs that can testify to two acts of pyrite formation).

Within the peculiarities of the pyrite thermoelectric properties from the Tukalo ore manifestation it was possible to distinguish two pyrite generations (pyrite I and pyrite II).

The pyrite thermoelectric properties data indicate one of the criteria for revealing pyrite generations (pyrite I and pyrite II) [11].

The thermo-e.m.f. and selection range of thermoelectric properties of the pyrite from the Kamin-Kliovka ore manifestation has its own characteristics (Tab. 7).

**Table 5.** Thermoelectrical properties of the pyrite crystals from the Tukalo ore manifestation (on its faces and inner parts)

Crystal number	Selection	Investigated simple forms that determine crystal habit	$\alpha$ [mcV/deg]			Selection range [mcV/deg]
			max.	min.	average	
1	b	cube and octahedron combination	+470	+200	+275	270
	a	crystal inner parts	+70	-50	-15	120
2	b	on the cube faces	+300	+10	+215	290
	a	crystal inner parts	+70	-110	+1	180
3	a	on the octahedron faces	-20	-110	-60	90
	c	cube and octahedron combination	-20	-100	-50	80
	b	crystal inner parts	+70	-70	-5	140
4	b	cube and octahedron combination	-20	-110	-60	90
	a	crystal inner parts	+70	-200	-57	270
5	b	cube and octahedron combination	+630	+380	+460	250
	a	crystal inner parts	+470	+220	+360	250
6	b	cube and octahedron combination	+250	+20	+80	230
	a	crystal inner parts	+480	+210	+345	270
	d	cube and octahedron combination	+110	-60	+15	170
	c	crystal inner parts	+390	+100	+245	290
7	b	cube and octahedron combination	-20	-260	-145	240
	a	crystal inner parts	+570	+100	+336	470
8	b	cube with a striation on the faces	+690	+400	+490	290
	a	crystal inner parts	+720	+430	+565	290
9	a	cube	-50	-260	-240	210
	b	octahedron	-200	-280	-240	80

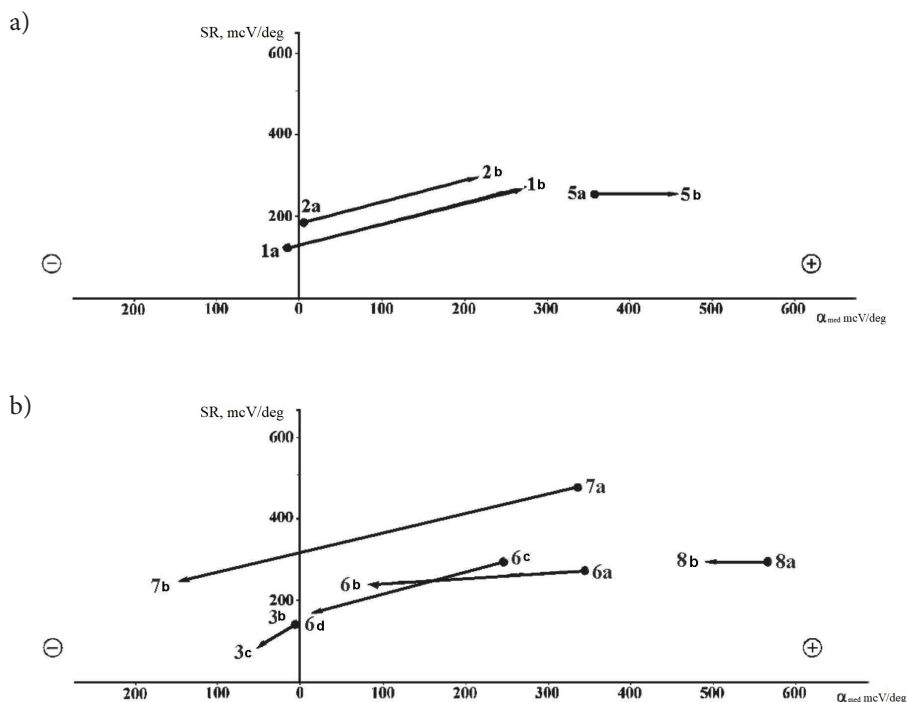


**Fig. 6.** Vectors of thermo-e.m.f. average values alterations and selections range of the pyrite I (a) and pyrite II (b) crystal growth vectors from the central parts of crystals to their surface (Tukalo ore manifestation, Rakhiv region)

**Table 6.** Thermoelectric properties (in faces and inner parts) of the pyrite crystals from the Sauliak deposit

Crystal number	Selection	Investigated simple firms that determine crystal habit	$\alpha_{med}$ [V/deg]			Selection range [mcV/deg]
			max.	min.	$\alpha_{med}$	
1	2	3	4	5	6	7
1/8	a	pentagonal dodecahedron	+400	+20	+165	380
	c	inner part	-20	-280	-140	260
	b	octahedron	+460	+200	+325	260
1	a	cube + octahedron	-20	-200	-60	180
	b	inner part	+90	-90	-25	180
6	a	cube with striation	-210	-460	-290	250
	c	inner part	-20	-220	-80	200
	b	octahedron	-6	-110	-45	105
38	a	cube with striation	-35	-280	-185	245
	b	octahedron	-20	-110	-90	90
	c	inner part	+90	-100	-25	190
40	a	cube	-20	-220	-80	200
	b	octahedron	+260	+20	+80	240
	c	inner part	+8	-250	-60	242
41	a	cube	+210	-90	+25	300
	b	inner part	+330	-70	+80	400
42	a	cube + octahedron + pentagonal dodecahedron	-20	-110	-70	90
43	a	cube with striation	+490	+340	+450	150
	b	inner part	+690	+210	+452	480
44	a	pentagonal dodecahedron	+680	+400	+540	280
	b	octahedron	+490	+240	+410	250
	c	inner part	+490	+200	+356	290
45	a	pentagonal dodecahedron	+660	+350	+535	310
	b	octahedron	+490	+260	+410	230
	c	inner part	+460	+280	+380	180

**Table 7.** Thermoelectric properties of the pyrite grains from the Kamin-Kliovka deposit

No.	Samples	$\alpha$ min.	$\alpha$ max.	$\alpha$ average	Selection range [mcV/deg]
1	1.	250	620	428.6	370
2	2	150	520	335.6	370
3	3	260	440	379.2	180
4	97/10 a	130	400	280.4	270
5	97/10 b	170	450	347	280
6	97/25 a	140	420	253.4	280
7	97/25 b	220	410	195.9	388
8	97/25 p/3	150	300	165.1	285
9	97/p/3 a	-290	-370	135.2	341
10	97/25 p/4	140	340	251.4	200
11	97/25p/5	40	380	266.4	340
12	97/25 p/6	40	350	210.4	310
13	97/25 p/7	-14	-450	265.8	436

## 4. Discussion

The Lostun ore manifestation presents two pyrite generations (pyrite I and pyrite II) as revealed by this investigation. The crystals belonging to the generations differ morphologically quite vividly (pyrite I has the form of a pentagonal dodecahedron, while pyrite II takes the form of a cube) and have different thermoelectrical properties. Pyrite I is widespread in ore bodies and enclosed rocks and is one of the earliest sulfides. In comparison, the spread of pyrite II is more restricted yet occurs more often than other sulfides (in particular galenite and chalcopyrite). This mineral mainly occurs in the form of monocrystalline formations that are often crushed and etched by later pyrite II separations. The main habit form of its crystals is that of a pentagonal dodecahedron which is sometimes partially ferruginated. Pyrite II has a classic yellow and sometimes light yellow color. Its crystals are sometimes ferruginated. With pyrite II separations, mono crystals predominate over other forms, with the occurrence of growth, aggregates and streaks of different forms and sizes (from 0.2 to 1.5 mm). It must be noted that pyrite II cubic crystals have vividly expressed stunting on their faces in the quartz-carbonate streaks. Their generations, in association with galenite or chalcopyrite in some sections, take the form of thin streaks or separations of an irregular form. The pyrite II thermoelectrical properties results testify to the fact that this mineral has only hole-conductivity.

With the Tukalo and Kamin-Kliovka ore manifestations, pyrite I has a habitual form which is mainly determined by octahedron faces as well as combina-

tion of cubes and octahedrons. As a rule, the octahedron faces of the investigated crystals almost always have flat shimming surface. Poikilitic enclosures of chalcopyrite, galenite and sphalerite sometimes occur in pyrite I connected with crossing fissures that corrode pyrite I crystals. The presence of these minerals and native gold were ascertained by the growth zones of pyrite I. This mineral is mainly spread throughout enclosed rocks (with a thin noncontinuous ferruginization film) but also occur in compositions of quartz and quartz-carbonate veins and streaks. The habitual form of pyrite II crystals are determined by a combination of cubes and octahedrons. Pyrite II crystals aspire to selvages of the quartz and quartz-carbonate veins and streaks. The sizes of its crystals are mainly 0.2–2.0 mm; they also have a flat surface, sometimes with a blocky structure or uneven striation of the surface of the faces.

## 5. Conclusions

The Chyvchyny and Rakhiv ore regions have some common features of geological structure (structural-tectonic, petrological, lithology-stratigraphic [1–5]. Their structural-metallgenetic position is caused by belonging to the Chyvchyny and Rakhiv outcrops of the Marmarosky massif. The single-type ore-bearing formations are spread within its boundaries.

Thus, in terms of the general thermo-e.m.f. as well as a selection range of the thermoelectric properties of the pyrite from the Lostun, Kamin-Kliovka, and Tukalo

ore manifestations and the Sauliak auriferous deposit are similar (in particular, by statistically reliable selections of thermo-e.m.f. values investigated crystals possess electron, hole or mixed conductivity; at the same time, these meanings are clearly grouped into two massifs that testifies to two acts of pyrite formation).

The comparative character of the thermoelectric properties of the pyrite from the investigated ore manifestations, the Sauliak deposit (see Figs. 2–4) and other auriferous deposits [12–14] testify to the supra-ore level of gold mineralization in the Tukalo and Lostun objects and make it possible to assume that the erosion shear of the gold mineralization in the Tukalo ore manifestation is similar to the Sauliak deposit erosive shear and is deeper in comparison with the Lostun ore manifestation; at the same time, a more reliable estimation of

the deep horizons of the investigated ore manifestations can be realized after a detailed thermobarogeochemical study of the productive complexes of the minerals within these ore manifestations.

**Funding:** This research received no external funding. The article was carried out within the framework of the project “The origin of ore-bearing processes in the lithologic association to the Carpathians region” No. 0117U000891 (<https://nddkr.ukrintei.ua/>).

**Acknowledgments:** We thank O.O. Nechepurenko (Rakhiv geological and exploratory party), Prof. I.V. Popivnyak, Prof. S.I. Tsikhon', V.P. Marusyak, and T.P. Oliynyk for their help and assistance in our visits and observations of the Rakhiv region deposits.

## References

- [1] Boyko A.K.: *Doverkhnepaleozoyskiy kompleks severo-zapadnogo okonchaniya Marmaroshskogo massiva (Vostochnyye Karpaty)*. LDU, Lvov 1970 [Бойко А.К.: *Доверхнепалеозойский комплекс северо-западного окончания Мармарошского массива (Восточные Карпаты)*. ЛДУ, Львов 1970].
- [2] Gabinet M.P., Kul'chitskiy Ya.O., Matkovskiy O.I., Yasinskaya A.A.: *Geologiyai poleznyye iskopayemyye Ukrain-skikh Karpat. Chast' 2. Tektonika, voprosy litogeneza, magmatizma i metamorfizma, zakonoternosti razmesh-cheniya polezny.* Vyshcha Shkola, Lvov 1977 [Габинет М.П., Кульчицкий Я.О., Матковский О.И., Ясинская А.А.: *Геология и полезные ископаемые Украинских Карпат. Часть 2. Тектоника, вопросы литогенеза, магматизма и метаморфизма, закономерности размещения полезных ископаемых*. Выща Школа, Львов 1977].
- [3] Gabinet M.P., Kul'chitskiy Ya.O., Matkovskiy O.I.: *Geologiyai poleznyye iskopayemyye Ukrain-skikh Karpat. Chast' 1. Stratigraficheskiy i litologo-geokhimicheskiy ocherk.* Vyshcha Shkola, Lvov 1976 [Габинет М.П., Кульчицкий Я.О., Матковский О.И.: *Геология и полезные ископаемые Украинских Карпат. Часть 1. Стратиграфический и литолого-геохимический очерк*. Выща Школа, Львов 1976].
- [4] Lazarenko Ye.K., Habinet M.P., Slyvko Ye.M.: *Mineralohiya osadochnykh utvoren' Prykarpattya*. LDU, Lviv 1962 [Лазаренко Є.К., Габинет М.П., Сливко Є.М.: *Мінералогія осадових утворень Прикарпаття*. ЛДУ, Львів 1962].
- [5] Matkovskiy O.I.: *Mineralogiya i petrografiya Chivchinskikh gor.* LGU, Lvov 1971 [Матковский О.И.: *Минералогия и петрография Чивчинских гор*. ЛГУ, Львов 1971].
- [6] Tsikhon' S.I.: *Tipomorfnyye osobennosti raznovozrastnykh generatsiy pirita rudoproavleniya Belopotokskoye.* In: *Tez. dokl. IX Mezhdunar. konf. po termobarogeokhimii, 18–22 oktyabrya 1999.* Aleksandrov 1999, pp. 201–202 [Цихонь С.И.: *Типоморфные особенности разновозрастных генераций пирита рудопроявления Белопотокское*. В: *Тез. докл. IX Междунар. конф. по термобарогеохимии, 18–22 октября 1999*. Александров 1999, с. 201–202].
- [7] Tsikhon' S.I., Popivnyak I.V., Marusyak V.P., Oliynyk T.P.: *Typomorfni osoblyvosti pirytu Rakhivshchyny ta Chyvchyn.* Visnyk Lvivs'koho universytetu. Seriya heolohichna, vup. 15, 2001, pp. 93–103 [Цихонь С.И., Попівняк І.В., Марусяк В.П., Олійник Т.П.: *Типоморфні особливості піриту Рахівщини та Чивчин*. Вісник Львівського університету. Серія геологічна, вип. 15, 2001, с. 93–103].
- [8] Marusyak V.P.: *Termoelektrychni blastostyli ta formy millennialny pirytu iz kvartsovykh zhyl ta vmisnykh porid rudo-proyavu Dobryn (Chyvchyns'ki hory).* In: *Suchasni problemy litolohiyi: Materialy nauk. konf., prysvyach. 100-rich-chyu vid dnya narodzh. D.P. Bobrovnyuka.* Lviv 2000, pp. 25–35 [Марусяк В.П.: *Термоелектричні властивості та форми виділення піриту із кварцових жил та вмісних порід рудопрояву Добрин (Чивчинські гори)*. В: *Сучасні проблеми літології: Матеріали наук. конф., присвяч. 100-річчю від дня народж. Д.П. Бобровника*. Львів 2000, с. 25–35].

- [9] Marusyak V., Kostyuk O., Byrych O., Oliynyk T., Popivnyak I.V. Tsikhon' S.I.: *Mineralohichna charakterystyka ta termoelektrychni vlastyvoli sul'fidiv zoloto-polimetalichnoho rudo proyavu Kamini'-Klovka*. In: *Naukovi osnovy prohnozuvannya, poshukiv ta otsinky rodovyshch zolota: Materialy przerozumovany. nauk. konf., Lviv, 27-30 veres. 1999 r.* Lviv 1999, pp. 79-80 [Марусяк В., Костюк О., Бирич О., Олійник Т., Попівняк І.В. Ціхонь С.І.: *Мінералогічна характеристика та термоелектричні властивості сульфідів золото-поліметалічного рудо прояву Камінь-Кльовка*. В: *Наукові основи прогнозування, пошуків та оцінки родовищ золота: Матеріали міжнар. наук. конф., Львів, 27-30 верес. 1999 р.* Львів 1999, с. 79-80].
- [10] Marusyak V.P., Oliynyk T.P., Tsikhon' S.I., Popivnyak I.V.: *Termoelektrychni vlastyvoli pirytu (Chyvchyna i Rakhivshchyna)*. Visnyk Lvivs'koho universytetu. Seriya heolohichna, vup. 16, 2002, pp. 116-126 [Марусяк В.П., Олійник Т.П., Ціхонь С.І., Попівняк І.В.: *Термоелектричні властивості піриту (Чивчини і Рахівщина)*. Вісник Львівського університету. Серія геологічна, вип. 16, 2002, с. 116-126].
- [11] Shafranovskiy I.I.: *Leksii po kristallomorfologii*. Vysshaya Shkola, Moskva 1968 [Шафрановский И.И.: *Лекции по кристалломорфологии*. Высшая Школа, Москва 1968].
- [12] Popivnyak I.V.: *Ob ispol'zovanii tipomorfnykh priznakov pirita v poiskovoy i otsenochnoy praktike*. Mineralohichnyy zbirnyk, no. 30, vip. 1, 1976, pp. 116-126 [Попівняк І.В.: *Об использовании типоморфных признаков пирита в поисковой и оценочной практике*. Мінералогічний збірник, № 30, вип. 1, 1976, с. 116-126].
- [13] Rakcheyev A.D.: *Zavisimost' sostava i svoystv piritov ot usloviy ikh obrazovaniya*. In: *Novyye metody ispol'zovaniya mineralov igornykh porod*. MGU, Moskva 1973, pp. 5-11 [Ракчеев А.Д.: *Зависимость состава и свойств пиритов от условий их образования*. В: *Новые методы использования минералов и горных пород*. МГУ, Москва 1973, с. 5-11].
- [14] Kostyuk O.V.: *Termoelektrychni vlastyvoli diahenetychno pirytu u vidkladakh paleotsenu (Skybova zona Ukrayins'kykh Karpat)*. Mineralohichnyy zbirnyk, no. 70, vup. 1-2, 2020, pp. 54-59 [Костюк О.В.: *Термоелектричні властивості діагенетичного піриту у відкладах палеоцену (Скибова зона Українських Карпат)*. Мінералогічний збірник, № 70, вип. 1-2, 2020, с. 54-59].